Comparison of multi-leaf collimator tracking and treatment-couch tracking during stereotactic body radiation therapy of prostate cancer

Ehrbar, Stefanie ; Schmid, Simon ; Jöhl, Alexander ; Klöck, Stephan ; Guckenberger, Matthias ; Riesterer, Oliver ; Tanadini-Lang, Stephanie

Abstract: PURPOSE AND BACKGROUND: Motion mitigation during prostate stereotactic body radiation therapy (SBRT) ensures optimal target coverage while reducing the risk of overdosage of nearby organs. The geometrical and dosimetrical performance of motion mitigation with the multileaf-collimator (MLC tracking) or the treatment couch (couch tracking) were compared. MATERIAL AND METHODS: For ten prostate patients, SBRT treatment plans with integrated boosts were prepared using volumetric modulated arc technique. For the geometrical evaluation, a lead sphere at the beam isocenter was moved according to five prostate motion curves (i) without mitigation, (ii) with MLC tracking or (iii) with couch tracking. During irradiation, MV images were taken and the over-/underexposed areas were evaluated. For the dosimetrical evaluation, the plans were applied to a dosimetric phantom. Dose distributions with and without mitigation were evaluated inside the target structure and organs at risk. RESULTS: The median over-/underexposed area was reduced significantly from 2.02cm2 without mitigation to 1.00cm2 and 0.45cm2 with MLC and couch tracking. Closest dosimetrical agreement to the static references was achieved with couch tracking. CONCLUSIONS: MLC and couch tracking at a conventional linear accelerator significantly improved the accuracy of prostate SBRT in the presence of motion, whereby couch tracking showed slightly better performance than MLC tracking.

DOI: https://doi.org/10.1016/j.radonc.2017.08.035

Received Date: 24 May 2017
Revised Date: 18 August 2017
Accepted Date: 29 August 2017

Title page

Proposed journal: Radiotherapy and Oncology

Comparison of multi-leaf collimator tracking and treatment-couch tracking during stereotactic body radiation therapy of prostate cancer

Stefanie Ehrbar[1], Simon Schmid[1], Alexander Jöhl[1,2], Stephan Klöck[1], Matthias Guckenberger[1], Oliver Riesterer[1], Stephanie Tanadini-Lang[1]

[1] *Department of Radiation Oncology, University Hospital Zurich and University of Zurich, Switzerland*
[2] *Product Development Group Zurich, Department of Mechanical and Process Engineering, ETH Zurich, Switzerland*

[+] *Corresponding author:* *Department of Radiation Oncology*
University Hospital Zurich
Rämistrasse 100
CH-8091 Zurich
stefanie.ehrbar@usz.ch

Key words: Prostate cancer, motion mitigation, couch tracking, MLC tracking, prostate motion, stereotactic body radiation therapy

doi: 10.1016/j.radonc.2017.08.035

Abstract

Purpose and Background: Motion mitigation during prostate stereotactic body radiation therapy (SBRT) ensures optimal target coverage while reducing the risk of overdosage of nearby organs. The geometrical and dosimetrical performance of motion mitigation with the multileaf-collimator (MLC tracking) or the treatment couch (couch tracking) were compared.

Material and Methods: For ten prostate patients, SBRT treatment plans with integrated boosts were prepared using volumetric modulated arc technique. For the geometrical evaluation, a lead sphere at the beam isocenter was moved according to five prostate motion curves (i) without mitigation, (ii) with MLC tracking or (iii) with couch tracking. During irradiation, MV images were taken and the over-/underexposed areas were evaluated.

For the dosimetrical evaluation, the plans were applied to a dosimetric phantom. Dose distributions with and without mitigation were evaluated inside the target structure and organs at risk.

Results: The median over-/underexposed area was reduced significantly from 2.02 cm^2 without mitigation to 1.00 cm^2 and 0.45 cm^2 with MLC and couch tracking. Closest dosimetrical agreement to the static references was achieved with couch tracking.

Conclusions: MLC and couch tracking at a conventional linear accelerator significantly improved the accuracy of prostate SBRT in the presence of motion, whereby couch tracking showed slightly better performance than MLC tracking.

Introduction

Active motion mitigation during radiotherapy treatments of moving targets can be used to reduce the high-dose treatment volume and thereby spare the healthy tissue. Stereotactic body radiation therapy (SBRT) has been shown to be an effective treatment for localised prostate cancer [1], however it could further profit from on-line motion mitigation. First, the prostate shows systematic and erratic motion which can reach up to 10 mm [2, 3, 4]. This motion is conventionally considered by increasing the target volume with a safety margin, but this simultaneously increases the dose to the adjacent organs. With on-line motion mitigation throughout the treatment, this margin could be reduced. Second, SBRT aims to deliver high target doses with steep dose gradients in only a few treatment fractions. To maximally exploit SBRT, high accuracy in dose delivery is required.

On-line motion mitigation can be performed at a conventional linear accelerator either by following the target motion with the treatment field through constant adaptation of the multileaf-collimator (MLC tracking [5, 6]), or by counter-movement of the patient with the treatment couch according to the target motion (couch tracking [7, 8]).

Studies on prostate treatment improvement have been performed for MLC tracking [9, 10] and couch tracking [11]. Moreover, both have been compared in a few studies. A multi-institutional study [12] compared real-time adaptive therapy with robotic, gimbaled, MLC and couch tracking. The four modalities were found to perform similarly. Other studies [13, 14] compared MLC and couch tracking directly for prostatic motion traces. They found better motion mitigation for couch tracking, especially for high-modulated treatment plans [13].

These studies focused their evaluation on the target dose distribution of a few treatment plans with a homogeneous dose prescription. For an extensive comparison of MLC and couch tracking, we included dosimetry of the nearby organs, a two level dose prescription and a larger patient cohort in combination with various distinct motion trajectories.

Material and Methods

Treatment planning

For ten prostate cancer patients, SBRT treatment plans with integrated boost to the index lesion were generated as described in Ehrbar et al. [11] using volumetric-modulated arc therapy (VMAT). A mean dose of 5 x 8 Gy = 40 Gy was prescribed to the planning target volume (PTV) around the index lesion (PTV_{index} = index lesion plus 3-mm margin), and a lower dose of 5 x 7 Gy = 35 Gy to the PTV around the prostate ($PTV_{prostate}$ = prostate plus 5 mm). Rectum, bladder and urethra were contoured as organs at risk (OAR). The rectum, bladder and urethra maximum dose (D0.1cc) was restricted to 36.25 Gy and the distal rectum wall to maximal 35 Gy. To test whether the tracking performance also depends on the MLC

orientation, two treatment plans were created for each patient, one with collimator rotations around 0° (range: 350°-10°) and one with 90° (80°-100°).

Motion traces

Five prostate motion traces were selected to show a variety of possible prostate displacements during radiotherapy treatments (see Ehrbar et al. [11] for details). These traces were recorded by Ehrbar et al. [11] (Trace 1) and Langen et al. [13] (Trace 2-5). The used sections of the traces are shown in **Figure 1** together with the temporal displacement fraction and mean offset for each motion trace.

MLC and couch tracking

Active motion mitigation with MLC or couch tracking was performed at a TrueBeam 2.0 linear accelerator (Varian Medical Systems, Inc., Palo Alto CA, USA). The TrueBeam was equipped with the High Definition 120 Leaf MLC and the PerfectPitch treatment couch. The system was employed in developer mode using the iTools-Tracking platform. This platform links the real-time position information of the target with the supervisor, which controls the MLC or couch position during the treatment. The position of the moving target was monitored with Calypso radiofrequency transponders (Varian Medical Systems, Inc., Palo Alto CA, USA) at a rate of 25 Hz and transferred to the iTools-Tracking software. A linear Kalman prediction filter is applied to the signal. For ongoing target motion, this filter is able to partially compensate for latencies caused by the time required for signal detection, signal processing and treatment adaptation. The predicted target displacement is then compensated with adaptation of the treatment field via the MLC or with counter-movement of the target via the treatment couch. The same tracking system was previously presented by Ehrbar et al. for couch tracking of lung tumors [15] and prostate tumors [11], and a similar system from the same vendor was studied by Hansen et al. [13] for MLC and couch tracking.

Geometrical performance

The geometrical performance of MLC and couch tracking was evaluated using mega-voltage (MV) fluoroscopy of a moving target. The target, a lead sphere with 10 mm diameter, was placed in the beam isocenter and moved in three dimensions with the HexaMotion stage (ScandiDos, Uppsala, Sweden). For position feedback, two Calypso transponders were placed on the lead sphere mount outside the treatment field. The twenty treatment plans were applied to the target and MV images were taken continuously at a rate of 7.7 Hz. These images show the lead sphere in respect to the MLC shaped field edges at different angular positions throughout the treatment. Each treatment plan was applied 16 times. First, one MV-image set was taken with the target in static position. This was used as the reference situation. Second, 15 MV-image sets were taken while the target was moved according to the five prostate motion traces during irradiation and with three modes of motion mitigation: no mitigation, MLC or couch tracking. The lead sphere was detected in each image with a template matching

algorithm (see **Figure 2**). The images were centered at the position of the lead sphere and a threshold was applied to create binary images. By comparison with the reference image at the same gantry angle, over- and underexposed areas at the field edges could be determined. This shows how well the motion was mitigated with MLC or couch tracking, since the relation between the lead sphere and the field edges should be the same for reference images and perfectly tracked images. Each measurement was quantified with the mean over-/underexposed area ($\bar{A}_{exposed}$) by averaging over the overexposed and underexposed areas of all images evaluated per MV image set.

Since the MV images were not taken exactly at the same gantry angles, the image sets were interpolated to every 1° of the treatment arc and only these interpolated images were taken into the evaluation. VMAT plans are highly modulated and might block the view of the lead sphere. Therefore, the MLC leafs of the treatment plan were artificially retracted by 60 mm. The artificially enlarged area was removed from the evaluation during image post-processing.

The reproducibility of the geometric measurement and evaluation algorithm was tested by comparing four repeated static measurements of patient 10 against the initial static measurement. Two reproducibility measurements were taken right after the initial static measurement and before the acquisition of mitigated measurements (pre-acquisition), while the other two reproducibility measurements were taken after all mitigated measurements (post-acquisition). The $\bar{A}_{exposed}$ of the pre- and post-acquisition reproducibility measurements, compared to the initial static measurements, were calculated.

Dosimetrical performance

The dosimetrical performance of MLC and couch tracking was evaluated using phantom measurements. The treatment plans were delivered to the Delta^4 phantom (ScandiDos, Uppsala, Sweden), which was mounted on the HexaMotion stage. For each treatment plan, 16 measurements were taken. First, one dose measurement was taken with the target in static position. This was used as reference situation. Second, 15 measurements were taken while the phantom was moved according to the five prostate motion traces during irradiation and with three modes of motion mitigation: no mitigation, MLC or couch tracking. The dose was measured in a biplanar array within the phantom and backprojected over the whole phantom using depth-dose curves. The patient's anatomical contours were overlayed to this dose distribution and dose parameters were compared against the static references. Gamma agreement indices (GAI) with 1%/1 mm and 2%/2 mm pass criterion were evaluated within the entire phantom, the target structures (index lesion and prostate) and the OARs (rectum, urethra, bladder). Global dose differences were used with the 100% dose level set at the maximum dose of the treatment plan, and only doses above 20% were taken into the gamma evaluation. For the target structures, the deviations in the mean dose (Dmean) and in the dose covering 95% of the volume (D95) were evaluated. For the OARs, the deviations in the

maximal dose (Dmax) were evaluated. For this organ specific evaluations, the research version 1.00.0103c of the Delta^4 dose evaluation software was used together with the Delta^{4DVH} function.

Data evaluation and statistics

The mean over-/underexposed area ($\bar{A}_{exposed}$) and the phantom $GAI_{2\%/2mm}$ were separately evaluated for all traces and collimator rotations. For the organ specific evaluations, the results of all measurements per mitigation mode were grouped together. Comparisons between collimator rotations or between mitigation modes were performed with a paired Wilcoxon signed rank test, while mitigation modes were compared with a multi-sample Friedman's test beforehand. The equality of variance was tested with multi-sample Brown Forsythe test, performing an ANOVA on absolute deviations of the data values from their group medians. This was done for the dose parameters only (Dmean, D95 and Dmax). Correlations between the geometrical and dosimetrical performance were evaluated with Spearman rank correlation coefficients (*Rho*). The significance level was set at 5% for all tests (p<0.05, for p-values multiplied with Bonferroni correction).

Results

Geometrical performance

Over all traces and collimator rotations, the median $\bar{A}_{exposed}$ was reduced significantly from 2.02 cm^2 (quartiles: 1.55 cm^2, 2.51 cm^2) without motion mitigation to 1.00 cm^2 (0.77 cm^2, 1.21 cm^2) and 0.45 cm^2 (0.40 cm^2, 0.54 cm^2) with MLC and couch tracking, respectively. **Figure 3A** shows the $\bar{A}_{exposed}$ separately for each motion trace, collimator rotation and mitigation mode. For the stable prostate (trace 5) all mitigation modes showed similar values. For all mitigation modes, the plans with 90° collimator rotation showed lower median $\bar{A}_{exposed}$ than 0°. This difference was significant for no mitigation (-0.33 cm^2) and couch tracking (-0.04 cm^2), but not for MLC tracking (-0.12 cm^2).

For the two pre-acquisition reproducibility measurements, $\bar{A}_{exposed}$ of 0.11 cm^2 and 0.16 cm^2 were found, and 0.24 cm^2 and 0.29 cm^2 for post-acquisition. For comparison, the median field openings per patient and arc were evaluated and ranged from 11.47 cm^2 to 26.27 cm^2 with a mean of 18.30 cm^2.

Dosimetrical performance

Over all traces and collimator rotations, the median phantom $GAI_{2\%/2mm}$ was improved significantly from 83.9% (quartiles: 77.0%, 94.1%) without motion mitigation to 98.6% (96.3%, 99.7%) and 100.0% (100.0%, 100.0%) with MLC and couch tracking, respectively. **Figure 3B** shows the $GAI_{2\%/2mm}$ separately for each motion trace, collimator rotation and mitigation mode. For all mitigation modes, the plans with 90° collimator rotation showed a better median

$GAI_{2\%/2mm}$ than 0°. This difference was significant for all, possibly relevant for no mitigation (+4.1%) and MLC tracking (+2.2%), but irrelevant for couch tracking (+0.0%).

The structure specific GAI and changes in dose parameters are shown in **Figure 4**. The corresponding values are presented in **Table 1** and comparisons between mitigation modes in **Table 2**. Overall, both tracking concepts resulted in better coverage of the target volumes and better agreement of the OAR doses than no mitigation. While the index lesion and prostate Dmean were significantly decreased without mitigation (median: -0.64% and -0.17%, respectively), Dmean showed a small difference to the static situation with couch tracking (+0.11% and +0.09%) and significantly increased values with MLC tracking (+0.22% and +0.49%). For the rectum and bladder, there was no significant difference found in Dmax between the mitigation modes, but the spread in the data was reduced with MLC and couch tracking. For the urethra, Dmax was significantly higher for MLC tracking (+1.05%) than couch tracking (+0.33%).

Over all parameters, the geometrical $\bar{A}_{exposed}$ was highly correlated (absolute *Rho* > 0.75*)* with the phantom, prostate, rectum, urethra and bladder $GAI_{1\%/1mm,}$ and the phantom, prostate and urethra $GAI_{2\%/2mm}$. The changes in dose parameters (ΔDmean, ΔD95 and ΔDmax) on the other hand showed only weak or no correlations with $\bar{A}_{exposed}$ (details see **Table 2**). But the variance of these dose parameters could be significantly reduced with couch tracking in all cases and with MLC tracking in most cases (see **Table 3**).

Discussion

Couch tracking and MLC tracking, two motion mitigation techniques at a conventional linear accelerator, were directly compared in this study. Both tracking concepts were able to improve the geometrical and dosimetrical accuracy of prostate SBRT in the presence of motion. The overall and organ specific evaluations showed good agreement with the static reference conditions for both mitigation techniques, with slightly better agreement for couch tracking.

For the geometrical evaluation, clinical treatment plans with realistic MLC modulation were used. The results showed significantly lower mean over- and underexposed area for couch tracking than MLC tracking (see **Figure 3**). Hansen et al. [13] performed a similar geometrical comparison, but used spherical field shapes without modulation. They showed better compensation with MLC tracking than couch tracking, except for small motions perpendicular to the MLC. This differential outcome might be explained by the missing MLC modulation in the simple spherical field: In modulated fields, more MLC leafs reach inside the open field than in a spherical field. The MLC tracking perpendicular to these MLC leafs is restricted due to the finite leaf width and their binary character. The MLC tracking error caused by the perpendicular motion component is therefore assumed to be larger for modulated fields with more complex field shapes. Additionally, the prostate motion traces show substantial motion in more than one direction, always resulting in a substantial motion component perpendicular to the leafs which

cannot be fully compensated. This might also explain why there was no relevant difference found between the two collimator rotations of 0° and 90°. However, Murtaza et al. [16] showed a reduced MLC tracking error for rotating collimator VMAT treatments, where the rotating collimator aligns the MLC leafs with the population-based dominant motion direction.

A further restriction of the investigated MLC tracking system might be its restricted maximum leaf speed of 25 mm/s. The MLC has two tasks, the dose modulation and the motion mitigation. By fulfilling both tasks simultaneously, the MLC might reach its physical restrictions. This could be solved by introducing a restriction in the maximum allowed MLC speed during treatment plan optimization.

The two tracking systems have different motion restrictions and therefore different tracking latencies. Those were reported by Hansen et al. [13] to be 146 ms for MLC tracking and 187 to 246 ms for couch tracking (depending on the period of a sinusoidal motion). These latencies are in the same range and might not influence the dosimetric results. Also due to the use of prediction filters, the dependence on the system latency might have been reduced.

Dosimetrically, the gamma agreement over the whole phantom with a 2%/2-mm criterion was improved from median 83.9% without mitigation to 98.6% with MLC tracking and to 100.0% with couch tracking. Better dosimetric performance of couch tracking over MLC tracking has previously been shown. Menten et al. [14] showed with film measurements for prostate step-and-shoot IMRT a gamma agreement (2%/2 mm) of 60.1% without compensation, 85.0% with MLC tracking and 95.3% with couch tracking. Hansen et al. [13] also showed for a high modulated prostate plan a better dosimetrical performance of couch tracking (failure rate: 0.1%) compared to MLC tracking (15.5%). The performance of MLC tracking in the present study was closer to couch tracking than in these previous studies. This might possibly be caused by different prediction filters and control loops, or by the thinner leaf width used in our study of only 2.5 mm compared to 5 mm.

The organ specific evaluation (see **Figure 4** and **Table 1**), showed that underdosage of the target volume and overdosage of the organs at risk can be mitigated successfully with tracking. Couch tracking showed very close agreement to the static reference measurements for all GAI and dose parameters. MLC tracking showed slightly worse agreement. Concretely, a dose increase above the static values was found for the target structures with MLC tracking. This increased target dose also resulted in increased urethra Dmax and explains the worse target and urethra $GAI_{1\%/1mm}$ for MLC tracking than couch tracking. The cause for these increased target doses is ambiguous. Probably, the field openings were increased during MLC tracking or the shifts of the field opening against the beam profile might have altered the actual photon fluence.

The geometrical performance agrees well with the gamma evaluations of the dosimetrical measurements (see correlations **Table 2**). However, the geometrical measure does not

satisfactorily correlate with the changes in the other dosimetrical parameters as changes in Dmean, D95 and Dmax. These low correlations might be explained by the dependence of these parameters on the motion direction rather than the total amount of target offset alone. Also the median changes in Dmax did not differ significantly. However, we showed that the variance of these parameters was significantly reduced with tracking and therefore tracking would benefit the overall patient cohort by minimizing the dose offset from the planned dose distribution.

The measurement reproducibility of the dosimetric evaluation was previously evaluated [11]. Repeated measurements showed perfect agreement with a 1%/1-mm gamma criterion. It was also shown that the Calypso system has no considerable influence on the dose measurement. To approximate the accuracy of the geometric measurements, the reproducibility was tested with five repeated static measurements showing an $\bar{A}_{exposed}$ of 0.11 cm^2 to 0.29 cm^2 (0.5% to 1.3%, in respect to the median field opening). These discrepancies might have been caused by the angle-wise interpolation of the fields or by inaccuracies of beam delivery itself. The geometric evaluations are assumed to be more sensitive to target offset, since every under-/overexposed pixel (0.021x0.021 cm^2) of each interpolated image is taken into consideration and not only the overall dosimetric effect. Generally, an $\bar{A}_{exposed}$ below 0.90 cm^2 showed $GAI_{2\%/2mm}$ above 95%.

The accuracy of the dosimetric evaluation depends directly on the accuracy of the Delta^4 dose measurement and its 3D interpolated dose. Latter has been validated with film measurements [17], ion chamber measurements [18] and a rotating phantom arrangement [19]. All three studies showed good agreement of the 3D interpolated dose with the independently measured dose and the planned dose. Furthermore, to exclude inaccuracies of dose calculation algorithms and measurement limitation from the tracking inaccuracies, comparisons were performed against measured dose distributions in static setup instead of the planned dose distributions.

In this study, only rigid motion of the prostate and the surrounding organs was assumed. For a more sophisticated evaluation regarding deforming tissues, either anthropomorphic dosimetric phantoms, which can perform realistic deformations, or dose reconstructions using four-dimensional image information are required. Latter could be realized with MRI-guided radiotherapy units, where continuous imaging information can be employed to reconstruct the dose to moving and deforming organs as proposed by Glitzner et al. [20]. The dynamic change of the beam (MLC tracking) or patient position (couch tracking) could easily be included into this dose accumulation workflow. Real-time 4D dose reconstruction for MLC tracking have been proposed [21, 22], but without including real-time images as calculation basis yet.

MLC and couch tracking can also be employed to compensate for respiratory motion, which has a different dynamic behavior than prostatic motion. On a dosimetric level, both tracking

techniques have been found to perform similarly for lung traces and improved the dose deposition accuracy when compared to no mitigation [13, 14].

The possibility of a hybrid couch-MLC tracking has been investigated by Toftegaard et al. [23] in a simulation study. A combination of both techniques would further improve the accuracy, when compared to pure MLC tracking, and simultaneously reduce the acceleration and jerk applied to the patient by the treatment couch, compared to pure couch tracking.

The results of this comparison study are valid for the presented MLC and couch tracking systems. The performance of couch and MLC tracking is generally limited by the accuracy of the motion signal, the system latency, the effectiveness of the prediction filter and hardware restrictions such as maximal speed and acceleration of the couch or MLC leafs and the MLC leaf width. Developments in these domains could further improve the tracking performance. A different tracking implementation might therefore change the results of this experiment.

To make tracking safely applicable in clinics, further work should be invested in quality assurance protocols, robustness analyses and the evaluation of inverse interplay effects of nearby organs which do not move according to the target structures.

Conclusion

In this study, MLC and couch tracking were found to significantly improve the geometrical and dosimetrical accuracy of hypo-fractionated prostate treatments, while couch tracking showed generally better performance than MLC tracking. Couch and MLC tracking are motion-mitigation techniques which can be implemented at conventional linear accelerators accessible to a large cohort of patients.

Acknowledgements

We would like to thank Kristijan Macek, Dieter Seghers and Vaclav Brandejsky for their technical support. This work was supported by the grant CR32I3_153491 of the Swiss National Science Foundation.

Disclosure of Conflicts of Interest

The authors have no relevant conflicts of interest to disclose.

References

[1] Henderson D, Tree A, van As N. Stereotactic body radiotherapy for prostate cancer. *Clinical Oncology.* 2015;27(5):270-79.

[2] Litzenberg DW, Balter JM, Hadley SW, et al. Influence of intrafraction motion on margins for prostate radiotherapy. *International Journal of Radiation Oncology* Biology* Physics*. 2006;2:548-53.

[3] Nederveen AJ, van der Heide UA, Dehnad H, van Moorselaar RJA, Hofman P, Lagendijk JJ. Measurements and clinical consequences of prostate motion during a radiotherapy fraction. *International Journal of Radiation Oncology* Biology* Physics*. 2002;1:206-14.

[4] Langen KM, Willoughby TR, Meeks SL, et al. Observations on real-time prostate gland motion using electromagnetic tracking. *International Journal of Radiation Oncology* Biology* Physics*. 2008;4:1084-90.

[5] Keall PJ, Kini V, Vedam S, Mohan R. Motion adaptive x-ray therapy: a feasibility study. *Physics in Medicine and Biology*. 2001;1:1.

[6] Keall PJ, Colvill E, O'Brien R, et al. The first clinical implementation of electromagnetic transponder-guided MLC tracking. *Medical physics*. 2014;2:020702.

[7] D'Souza D, Naqvi SA, Cedric XY. Real-time intra-fraction-motion tracking using the treatment couch: a feasibility study. *Physics in Medicine and Biology*. 2005;17:4021.

[8] Lang S, Zeimetz J, Ochsner G, Daners MS, Riesterer O, Klöck S. Development and evaluation of a prototype tracking system using the treatment couch. *Medical physics*. 2014;2:021720.

[9] Colvill E, Poulsen PR, Booth J, O'brien R, Ng J, Keall P. DMLC tracking and gating can improve dose coverage for prostate VMAT. *Medical physics.* 2014;41(9):091705.

[10] Colvill E, Booth JT, O'Brien R, et al. Multileaf collimator tracking improves dose delivery for prostate cancer radiation therapy: Results of the first clinical trial. *International Journal of Radiation Oncology*Biology*Physics*. 2015;5:1141-47.

[11] Ehrbar S, Schmid S, Jöhl A, et al. Validation of dynamic treatment-couch tracking for prostate SBRT. *Medical Physics.* 2017.

[12] Colvill E, Booth J, Nill S, et al. A dosimetric comparison of real-time adaptive and non-adaptive radiotherapy: A multi-institutional study encompassing robotic, gimbaled, multileaf collimator and couch tracking. *Radiotherapy and Oncology*. 2016;1:159-65.

[13] Hansen R, Ravkilde T, Worm ES, et al. Electromagnetic guided couch and multileaf collimator tracking on a TrueBeam accelerator. *Medical physics*. 2016;5:2387-98.

[14] Menten MJ, Guckenberger M, Herrmann C, et al. Comparison of a multileaf collimator tracking system and a robotic treatment couch tracking system for organ motion compensation during radiotherapy. *Medical physics*. 2012;11:7032-41.

[15] Ehrbar S, Perrin R, Peroni M, et al. Respiratory motion-management in stereotactic body radiation therapy for lung cancer – A dosimetric comparison in an anthropomorphic lung phantom (LuCa). *Radiotherapy and Oncology.* 2016;121(2):328-34.

[16] Murtaza G, Toftegaard J, Khan EU, Poulsen PR. Volumetric modulated arc therapy with dynamic collimator rotation for improved multileaf collimator tracking of the prostate. *Radiotherapy and Oncology.* 2017;122(1):109-15.

[17] Feygelman V, Forster K, Opp D, Nilsson, G. Evaluation of a biplanar diode array dosimeter for quality assurance of step-and-shoot IMRT. *Journal of Aplied Clinical Medical Physics.* 2009;10(4):64-78.

[18] Calvo O, Gutierrez A, Stathakis S, et al. SU-FF-T-386: Validation of the Delta4 Dosimetry Phantom Against Ionometric Measurements. *Medical Physics.* 2009;36(6):2610.

[19] Sadagopan R, Bencomo JA, Martin RL, Nilsson G, Matzen T, Balter PA. Characterization and clinical evaluation of a novel IMRT quality assurance system. *Journal of Applied Clinical Medical Physics.* 2009;10(2):104-19.

[20] Glitzner M, Crijns S, de Senneville BD, et al. On-line MR imaging for dose validation of abdominal radiotherapy. *Physics in medicine and biology.* 2015;60(22):8869.

[21] Poulsen PR, Schmidt ML, Keall P, Worm ES, Fledelius W, Hoffmann L. A method of dose reconstruction for moving targets compatible with dynamic treatments. *Medical physics.* 2012;39(10):6237-46.

[22] Fast M, Kamerling C, Ziegenhein P, et al. Assessment of MLC tracking performance during hypofractionated prostate radiotherapy using real-time dose reconstruction. *Physics in medicine and biology.* 2016;61(4):1546.

[23] Toftegaard J, Hansen R, Ravkilde T, Macek K, Poulsen PR. An experimentally validated couch and MLC tracking simulator used to investigate hybrid couch-MLC tracking. *Medical Physics.* 2017.

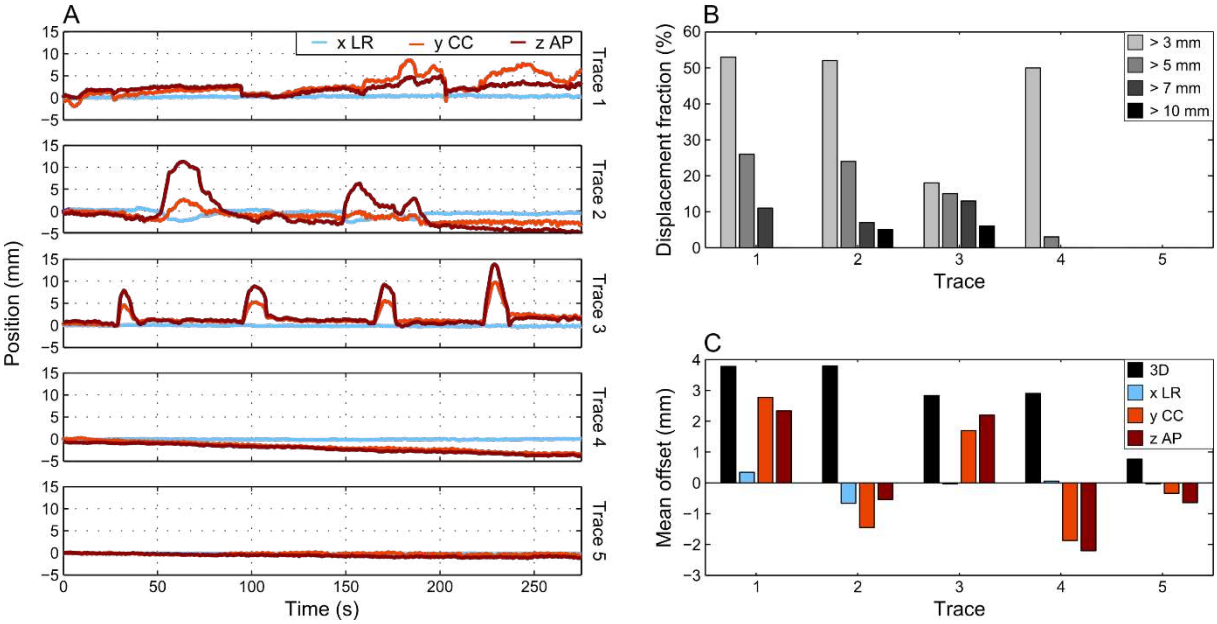

Figure 1: A) Sections of prostate motion traces (Trace 1-5). B) Temporal fraction of 3D prostate displacement larger than 3, 5, 7 and 10 mm. C) Mean values of the 3D, LR, CC and AP displacement for each trace.

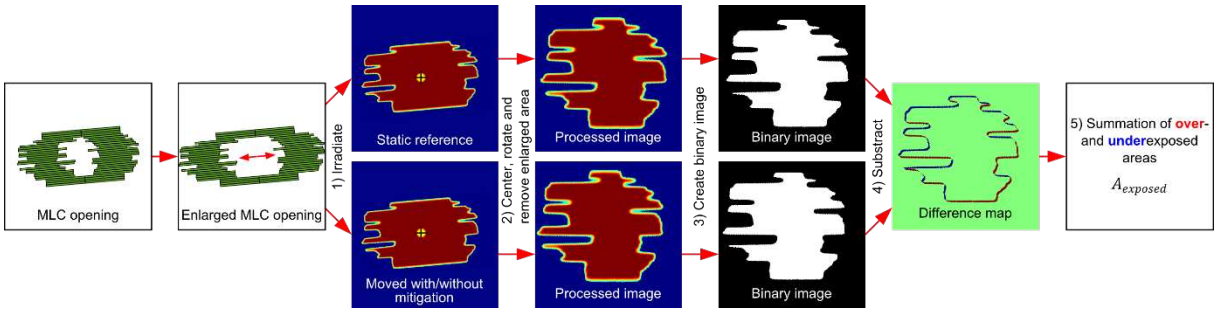

Figure 2: Schematic workflow of geometrical evaluation: 1) The artificially enlarged VMAT plans are applied and measured with the MV imager. 2) The center of the lead sphere is identified on the moved and static images and the artificially enlarged area is removed after rotating of the image. 3) Binary images are created by applying a threshold. 4) Both images are aligned and substracted. 5) Over- and underexposed areas at the field edges are summed up.

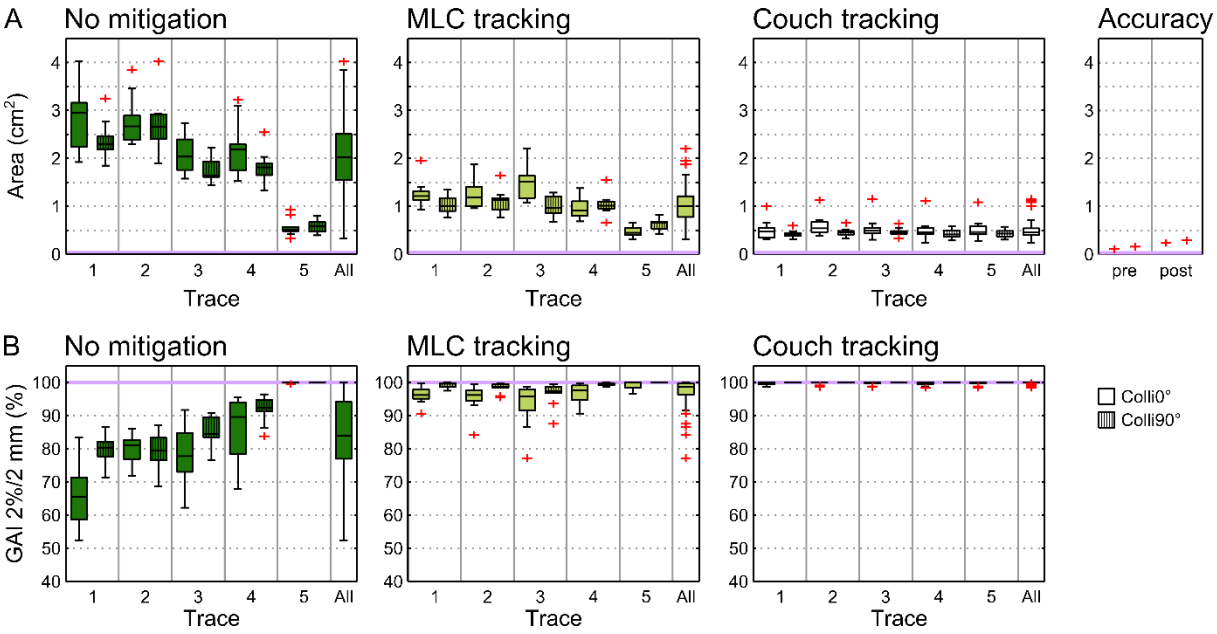

Figure 3: Geometrical and dosimetrical evaluation: Results are shown as boxplots over all patients for each motion trace (1-5) and collimator rotation (0° with plain box left, 90° with shaded box right at each trace), and for all measurements combined (All). A) The mean over- and underexposed area ($\bar{A}_{exposed}$) of all mitigation modes and of repeated static measurements of one patient pre- and post-acquisition (accuracy) B) The 2%/2-mm gamma agreement over the entire measurement phantom for doses larger than 20%.

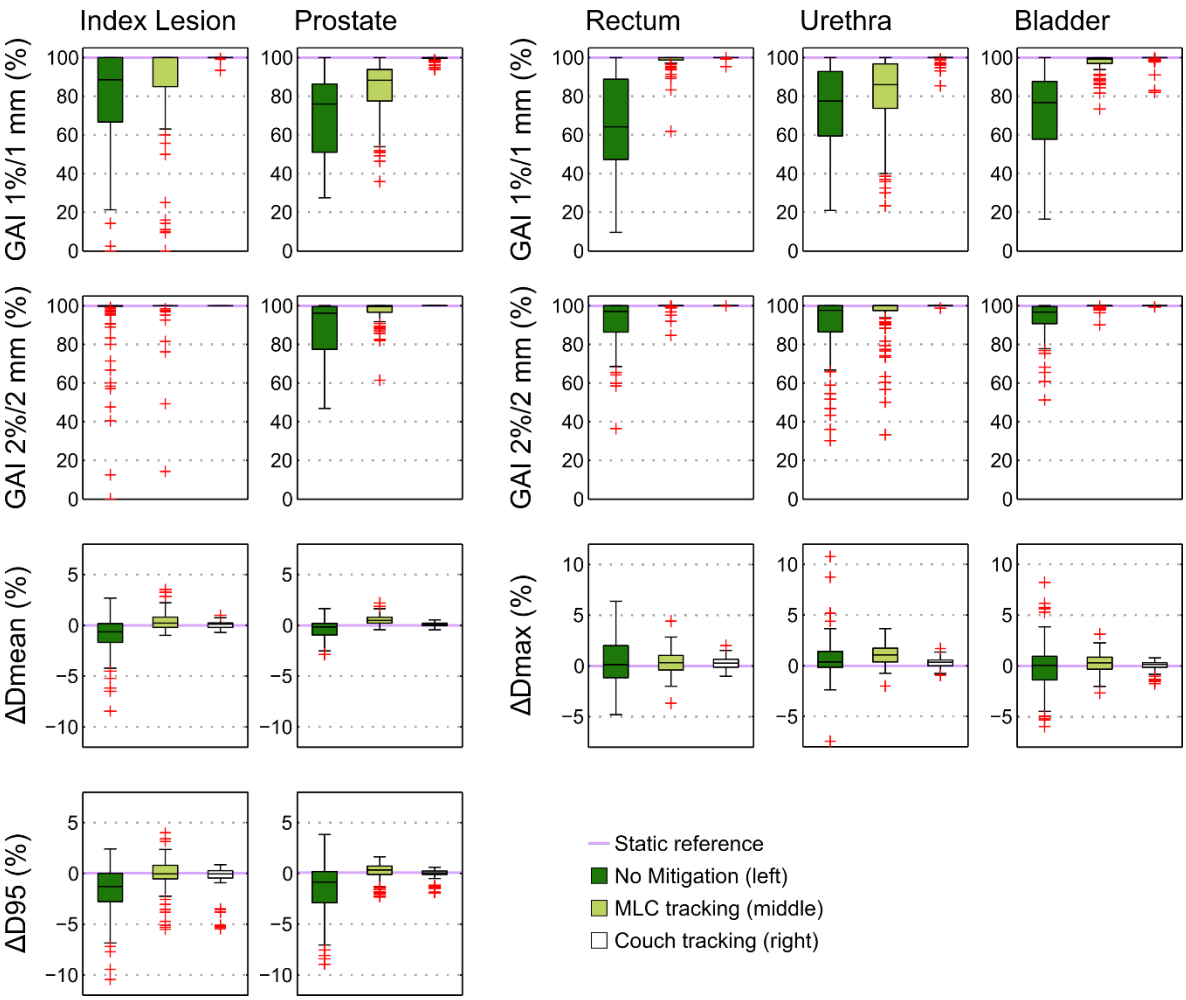

Figure 4: Organ specific dosimetrical evaluation: Results are shown as boxplots over all patients, motion traces and collimator rotations combined for the three mitigation modes: no mitigation (left in each plot), MLC tracking (middle) and couch tracking (right). Gamma agreement indices (GAI) with 1%/1-mm and 2%/2-mm criteria are shown for all structures, changes in the mean dose (ΔDmean) and the dose to 95% (ΔD95) for the target structures, and changes in maximum dose (ΔDmax) for the organs at risk. Δ: moved-static.

Table 1: Geometrical and dosimetrical evaluation. Median and quartiles of the over-/underexposed areas, gamma agreement indices and differences in dose parameters are given for each structure, showing the agreement with the static reference situation. Δ: moved-static.

Evaluation parameter	No mitigation Median (q25, q75)	MLC tracking Median (q25, q75)	Couch tracking Median (q25, q75)
$\bar{A}_{exposed}$ (cm²)	2.02 (1.55, 2.51)	1.00 (0.77, 1.21)	0.45 (0.40, 0.54)
Phantom			
GAI 1%/1mm (%)	53.6 (47.6, 65.8)	88.4 (80.9, 92.0)	99.2 (96.0, 100.0)
GAI 2%/2mm (%)	83.9 (77.0, 94.1)	98.6 (96.3, 99.7)	100.0 (100.0, 100.0)
Index lesion			
GAI 1%/1mm (%)	88.5 (66.7, 100.0)	100.0 (85.1, 100.0)	100.0 (100.0, 100.0)
GAI 2%/2mm (%)	100.0 (99.8, 100.0)	100.0 (100.0, 100.0)	100.0 (100.0, 100.0)
ΔDmean (%)	-0.64 (-1.69, 0.18)	0.22 (-0.20, 0.81)	0.11 (-0.21, 0.24)
ΔD95 (%)	-1.28 (-2.79, -0.00)	-0.05 (-0.54, 0.80)	-0.05 (-0.45, 0.27)
Prostate			
GAI 1%/1mm (%)	76.0 (51.1, 86.4)	88.2 (77.6, 93.9)	100.0 (99.5, 100.0)
GAI 2%/2mm (%)	96.2 (77.4, 99.5)	99.6 (96.6, 100.0)	100.0 (100.0, 100.0)
ΔDmean (%)	-0.17 (-0.95, 0.19)	0.49 (0.21, 0.81)	0.09 (-0.05, 0.28)
ΔD95 (%)	-0.86 (-2.88, 0.18)	0.32 (-0.09, 0.72)	0.05 (-0.09, 0.24)
Rectum			
GAI 1%/1mm (%)	64.2 (47.3, 88.9)	99.9 (98.8, 100.0)	100.0 (100.0, 100.0)
GAI 2%/2mm (%)	97.0 (86.4, 100.0)	100.0 (100.0, 100.0)	100.0 (100.0, 100.0)
ΔDmax (%)	0.12 (-1.16, 1.99)	0.32 (-0.41, 1.03)	0.23 (-0.13, 0.65)
Urethra			
GAI 1%/1mm (%)	77.5 (59.6, 92.9)	86.1 (73.8, 96.7)	100.0 (100.0, 100.0)
GAI 2%/2mm (%)	97.7 (86.5, 100.0)	100.0 (97.5, 100.0)	100.0 (100.0, 100.0)
ΔDmax (%)	0.35 (-0.16, 1.40)	1.05 (0.36, 1.73)	0.33 (-0.00, 0.57)
Bladder			
GAI 1%/1mm (%)	76.8 (57.8, 87.7)	99.3 (97.0, 99.8)	100.0 (99.9, 100.0)
GAI 2%/2mm (%)	96.7 (90.7, 99.5)	100.0 (99.9, 100.0)	100.0 (100.0, 100.0)
ΔDmax (%)	0.04 (-1.38, 0.94)	0.29 (-0.32, 0.86)	0.15 (-0.14, 0.32)

q25, q75: 25%- and 75%-percentiles

Table 2: Comparisons of motion mitigation modes with Friedman's test followed by Wilcoxon sign rank tests, and Spearman correlations of dosimetrical and geometrical results.

	Multiple-sample Friedman`s test	No mitigation vs MLC tracking	No mitigation vs Couch tracking	Couch vs MLC tracking	Spearman correalation with $\bar{A}_{exposed}$	
Evaluation parameter	*p*-value^{+}	*p*-value^{++}	*p*-value^{++}	*p*-value^{++}	*Rho*	*p*-value^{+++}
$\bar{A}_{exposed}$ (cm^2)	<0.001	<0.001	<0.001	<0.001	-	-
Phantom						
GAI 1%/1mm	<0.001	<0.001	<0.001	<0.001	-0.85	<0.001
GAI 2%/2mm	<0.001	<0.001	<0.001	<0.001	-0.87	<0.001
Index lesion						
GAI 1%/1mm	<0.001	0.191 ns	<0.001	<0.001	-0.64	<0.001
GAI 2%/2mm	<0.001	1.000 ns	<0.001	0.059 ns	-0.43	<0.001
ΔDmean	0.002	<0.001	<0.001	0.049	-0.23	<0.001
ΔD95	<0.001	<0.001	<0.001	0.242 ns	-0.24	<0.001
Prostate						
GAI 1%/1mm	<0.001	<0.001	<0.001	<0.001	-0.85	<0.001
GAI 2%/2mm	<0.001	<0.001	<0.001	<0.001	-0.84	<0.001
ΔDmean	<0.001	<0.001	<0.001	<0.001	-0.17	0.057 ns
ΔD95	<0.001	<0.001	<0.001	0.005	-0.31	<0.001
Rectum						
GAI 1%/1mm	<0.001	<0.001	<0.001	<0.001	-0.83	<0.001
GAI 2%/2mm	<0.001	<0.001	<0.001	0.003	-0.71	<0.001
ΔDmax	1.000 ns	1.000 ns	1.000 ns	1.000 ns	0.18	0.044
Urethra						
GAI 1%/1mm	<0.001	0.300 ns	<0.001	<0.001	-0.78	<0.001
GAI 2%/2mm	<0.001	0.463 ns	<0.001	<0.001	-0.62	<0.001
ΔDmax	<0.001	0.453 ns	1.000 ns	<0.001	0.15	0.192 ns
Bladder						
GAI 1%/1mm	<0.001	<0.001	<0.001	<0.001	-0.77	<0.001
GAI 2%/2mm	<0.001	<0.001	<0.001	0.009	-0.77	<0.001
ΔDmax	0.615 ns	1.000 ns	1.000 ns	0.687 ns	-0.06	1.000 ns

ns: not significant
p-values were adjusted according to Bonferroni correction (+/++/+++: multiplied by factor 20//60/19)
Rho: Spearman correlation coefficient

Table 3: Comparisons of motion mitigation modes with Brown-Forsythe test for equal variance.

Evaluation parameter	Multiple-sample Brown-Forsythe test *p*-value[+]	No mitigation vs MLC tracking *p*-value[++]	No mitigation vs Couch tracking *p*-value[++]	Couch vs MLC tracking *p*-value[++]
Index lesion				
ΔDmean	<0.001	<0.001	<0.001	<0.001
ΔD95	<0.001	0.051 ns	<0.001	1.000 ns
Prostate				
ΔDmean	<0.001	<0.001	<0.001	<0.001
ΔD95	<0.001	<0.001	<0.001	0.011
Rectum				
ΔDmax	<0.001	<0.001	<0.001	<0.001
Urethra				
ΔDmax	<0.001	0.196 ns	<0.001	<0.001
Bladder				
ΔDmax	<0.001	<0.001	<0.001	<0.001

ns: not significant
p-values were adjusted according to Bonferroni correction (+/++: multiplied by factor 7/21)